JOURNAL OF GEOPHYSICAL RESEARCH, VOL. 95, NO. C6, PAGES 9411–9420, JUNE 15, 1990

Hydrography and Microstructure of an Arctic Cyclonic Eddy

LAURIE PADMAN, MURRAY LEVINE, AND THOMAS DILLON

College of Oceanography, Oregon State University, Corvallis

JAMES MORISON

Applied Physics Laboratory, University of Washington, Seattle

ROBERT PINKEL

Scripps Institution of Oceanography, La Jolla, California

Hydrographic and velocity profiles were made through a small baroclinic cyclonic eddy during the Arctic Internal Wave Experiment in the Canada Basin in April 1985. The maximum measured azimuthal velocity was 0.38 m s^{-1} at a depth of 115 m, with velocities decaying to near zero at 30 and 270 m. Maximum isopycnal displacements at the closest approach to the eddy's axis were about 40 m. The deduced radius of maximum velocity is $r_0 = 7 \pm 2$ km, and the total radius is about 13 km. Kinetic energy dissipation rate, ε, was enhanced within 70 m of the surface throughout the transect, and for radius $r < r_0$ near 60 m and 180 m. The subsurface maxima in ε do not correspond to regions of low Richardson number, but are colocated with locally reduced shear, consistent with the observed dissipation rates being merely the remnants of recent, more energetic mixing events. The time scale for the decay of the eddy, based on its total energy and the measured dissipation rates, is $O(10)$ years. Given this large dissipation time scale, critical layer absorption of vertically propagating internal wave momentum may be dynamically significant to the eddy's evolution.

1. INTRODUCTION

The Arctic Internal Wave Experiment (AIWEX) was conducted from an ice camp drifting in the Canada Basin of the Arctic Ocean during March–May 1985. Velocity, temperature, and conductivity were sampled at fixed depths, and profiles of these variables from the surface to below 300 m were made. Toward the end of the experiment the camp drifted across a small eddy with a total inferred radius (see section 3.1) of about 13 km. From both the hydrographic data and current meter records, the rotation sense (parity) of the eddy was cyclonic, with an azimuthal velocity maximum near 115 m, decreasing to approximately zero near 30 m and 270 m. Small eddies are a common feature of the Canada Basin, being present in about 25% of the hydrographic and current meter profiles during the extensive Arctic Ice Dynamics Joint Experiment (AIDJEX) program in 1975/1976 [*Manley and Hunkins*, 1985]. They contain much of the kinetic energy in the depth range 0–250 m, and transport significant amounts of anomalous heat, salt, and nutrients within the Canada Basin. Understanding these eddies is therefore essential to modeling the upper ocean in the Canada Basin.

Manley and Hunkins [1985] found that approximately 95% of eddies identified during AIDJEX were anticyclonic. *Hunkins* [1974] documented one cyclonic eddy extending from near the surface to below 200 m from the AIDJEX pilot program in 1972. *Manley and Hunkins* [1985] found three cyclonic eddies during the main AIDJEX program in 1975–1976, but two of these were below the Atlantic layer core, i.e, below 500 m, while the third was very weak. *D'Asaro* [1988*a*], using helicopter-deployed expendable current profilers and conductivity, temperature, and depth (CTD) units, found two further cyclonic eddies below 300 m near the AIWEX camp. Therefore, while *McWilliams* [1988] claims that these small, isolated vortices are always anticyclonic, a total of seven cyclonic eddies have now been documented in the Canada Basin. However, the present observations are the first through a Canada Basin eddy of either parity that include high-resolution (both in space and time) current profiles and direct measurement of kinetic energy dissipation rate. Combined with hydrographic measurements, these observations allow us to investigate the energy balance of an eddy which is typical, in size and total energy, of those of the Canada Basin.

One of the intriguing features of these small eddies, or submesoscale coherent vortices (SCVs) [*McWilliams*, 1985], is their apparently long lifetimes, which are deduced from the estimated time taken for an eddy to travel from its proposed point of formation to the central Canada Basin. The present SCV and the majority of previously documented Arctic SCVs occur in the depth range $0 < z < 300$ m, which is the approximate range of the Canada Basin halocline, formed from Bering Strait summer and winter inflows and modified shelf water. This, combined with their typically anomalous water mass properties [*Manley and Hunkins*, 1985], suggests a probable formation point along the Alaska shelf. *D'Asaro* [1988*b*] proposed a mechanism for generation of anticyclonic eddies based upon the relative vorticity generated by frictional torques in a shear layer adjacent to the coastward wall of Barrow Canyon. He also hypothesized that the rarer cyclonic SCVs may be generated in a similar manner on the seaward wall of Barrow Canyon, and used satellite imagery of a patch of warm water near this wall to support this proposal.

Paper number 90JC00269.
0148-0227/90/90JC-00269$05.00

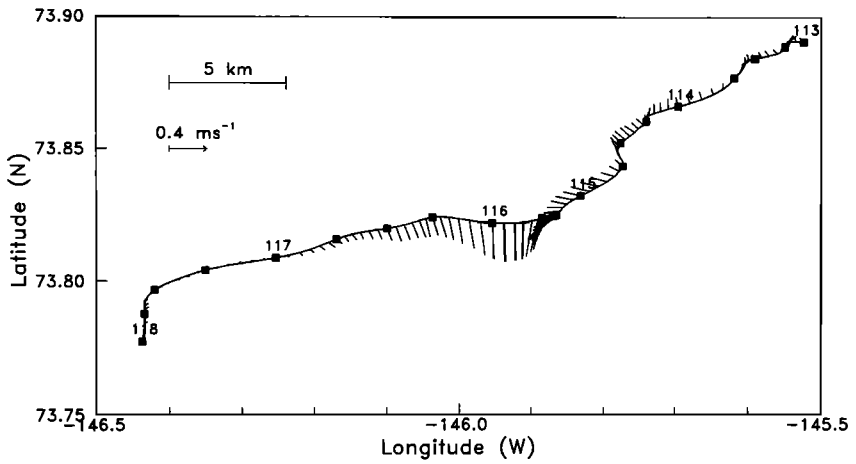

Fig. 1. Drift track for AIWEX ice camp, from t = 113.0 (UTC) to 118.0. Solid squares are separated by 6 h. Vectors indicate absolute currents at 115 m measured by ADCP.

An alternative mechanism is the growth via an instability process of meanders in the coastal current [*Griffiths and Linden*, 1982; *Killworth and Stern*, 1982]. As with D'Asaro's model, this mechanism favors generation of anticyclonic eddies because of the absence of a left-hand boundary to limit the growth of meanders in the offshore direction. However, under appropriate conditions, cyclonic eddies may be generated in this way by the near-simultaneous pinching off of two consecutive anticyclonic meanders. The wavelength of the growing instability, based on the work by *Griffiths and Linden* [1982], is $O(20)$ km for a 10-km-wide current in an upper layer 50 m deep in 1000 m total water depth, with a density contrast between layers of 2 kg m^{-3}, typical of the initial incursion of water from the Bering Strait into the Canada Basin. This implies an eddy radius of about 10 km, comparable to the observed scales of Canada Basin SCVs.

The assumption that SCVs are formed near the coast implies that these features are long-lived, since an eddy must move from the coast to the central Canada Basin without its vorticity field being erased. Even if the eddies follow a straight-line path from Point Barrow at an average speed of 0.02 m s^{-1}, a lifetime of several months is required. Much longer lifetimes are implied by more realistic paths, such as downstream (eastward) advection in the Alaska Coastal Current followed by westward advection in the southern branch of the anticyclonic Beaufort Gyre [*Newton et al.*, 1974]. It is a primary aim of this paper to explore the energy balance of the AIWEX cyclonic SCV in order to understand these long lifetimes in the presence of frictional losses both at the ice/water interface and through internal shear stresses.

Section 2 describes the hydrographic and velocity fields within the AIWEX camp eddy, then discusses observations of its microstructure. A description of AIWEX can be found in the work by *Padman and Dillon* [1987]. In section 3 we discuss the eddy geometry, and the relationship between the dissipation rate and eddy-scale hydrography. We also discuss the eddy's energy balance, and in particular the possibility that critical layer absorption of internal wave momentum flux may be a significant component of this balance.

2. Observations

The ice camp location (Figure 1) was obtained from a dual-channel Magnavox 1502 satellite navigator with a typical separation between good fixes of 1–2 h. The mean velocity of the camp was about 0.05 m s^{-1} roughly toward WSW, but variable between 0 and 0.12 m s^{-1} with large changes in direction, although the orientation of the ice floe remained almost constant. Throughout this paper, time t is given in decimal day of year (UTC). The relative locations of vertical profiles and moored sensors discussed in this paper are shown in Figure 2.

2.1. *Current Structure*

Horizontal velocity was recorded at 145 m by a vector-averaging current meter at the central mooring, and by an RD Instruments acoustic Doppler current profiler (ADCP) which measured good hourly averaged data between 30 and

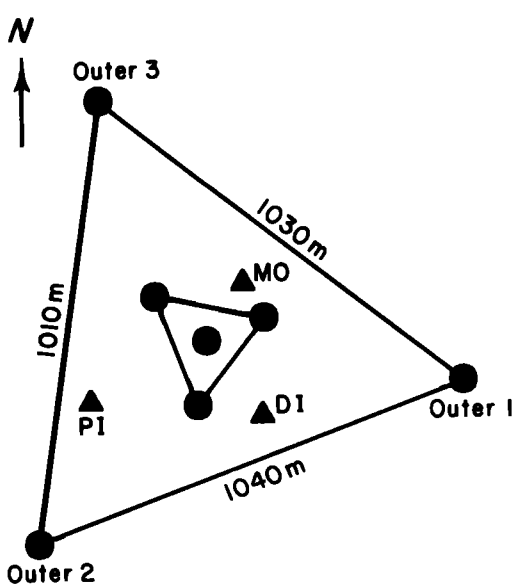

Fig. 2. Location of moored temperature sensors (solid circles) Arctic profiling system CTD (MO), acoustic Doppler current profiler (PI), and microstructure profiling (DI).

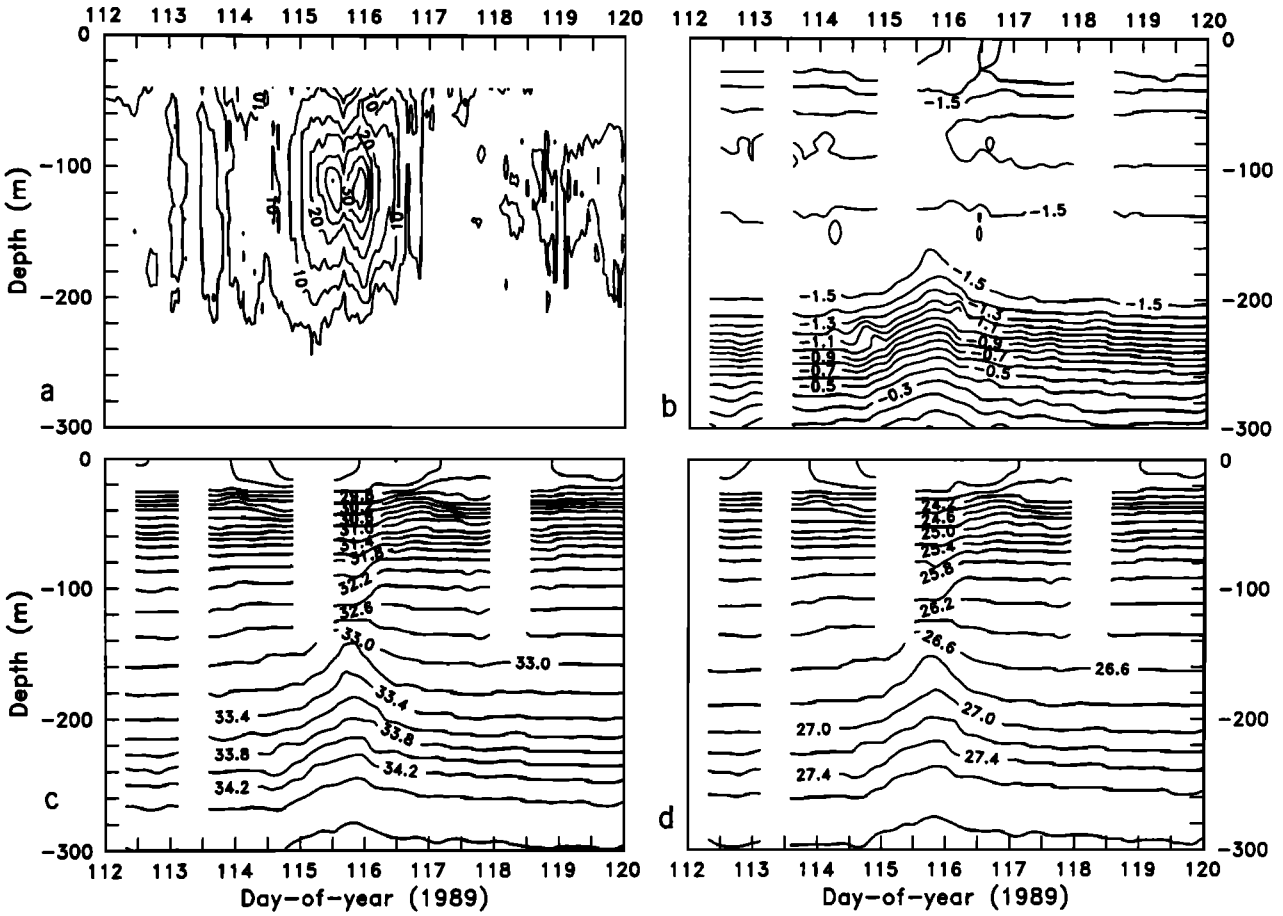

Fig. 3. Plots of (*a*) velocity magnitude, relative to 300 m depth, (*b*) temperature, T, (*c*) salinity, S, and (*d*) density, σ_t. Velocity is measured by acoustic Doppler current profiler with averaging scales of 8 m and 1 h; T, S, and σ_t are measured with the APS profiling CTD at an approximate sampling interval of 3 h.

300 m. The ADCP has a vertical resolution (separation of independent current estimates) of about 8 m, and an error in hourly averaged current speed, based on the assumption of zero vertical velocity, of about 3×10^{-3} m s^{-1}. The absolute velocity vectors at 115 m from the ADCP are shown in Figure 1. Outside the eddy, semidiurnal frequency oscillations are found in the current meter data, with typical magnitudes of 0.04 m s^{-1}. It is assumed that some of the signal within the eddy is also in this frequency band, which may be tidal or near-inertial ($2\pi/f$ = 12.48 h at 74°N). The velocity at 300 m, the deepest reliable ADCP current estimate, is assumed to represent a barotropic velocity consisting of tides superposed on the largescale Beaufort gyre circulation [*Newton et al.*, 1974], and has therefore been subtracted from the current profiles to produce a perturbation velocity field associated with the eddy. The perturbation velocity magnitude (Figure 3*a*) has two maxima of about 0.38 m s^{-1} at 115 m, at t = 115.5 and 116.0, with a decrease in speed between these times. The velocity field associated with the eddy is bounded approximately by $114.7 < t < 116.8$ and $30 < z < 270$ m.

2.2. *Hydrography*

Temperature, T, and conductivity, C, were measured at 1-min intervals at five depths between 80 and 508 m with Sea-Bird Electronics sensors on the central mooring [*Levine et al.*, 1986]. In addition, T was measured at about 250 m on six satellite moorings, designed as an antenna for internal wave phase propagation. Salinity, S, was obtained from T and C for averaging times longer than the conductivity cell flushing rate of several minutes. Hourly averages of T and S (Figure 4) show the eddy between about t = 114.7 and 116.8, with the closest approach to the eddy axis being near t = 115.7. The vertical lines indicate the times at which the 115-m current speed reached local maxima (see Figure 3*a*). The eddy is most clearly seen between 80 and 257 m. It is still evident at 303 m but is no longer observable at 508 m, which is near the core of the Atlantic layer. Transects of T, S, and σ_t (Figures 3*b*-3*d*) from the Arctic profiling system (APS) [*Morison et al.*, 1987] clearly show the depression of isopycnals associated with the eddy above 115 m, and the elevation of isopycnals below this depth. The T-S characteristics within the eddy vary slightly from the background (Figure 5). Prior to the eddy transect, the camp had crossed a field of small, localized lenses of anomalously cold water near 80 m [*Fields*, 1988; *Padman and Dillon*, 1988]: it is not known if these lenses are dynamically associated with the eddy.

2.3. *Dissipation Rates*

Seventy-five profiles of temperature and velocity shear microstructure were made with the rapid sampling vertical profiler [*Caldwell et al.*, 1985; *Padman and Dillon*, 1987], from the surface to a maximum depth of 460 m between t =

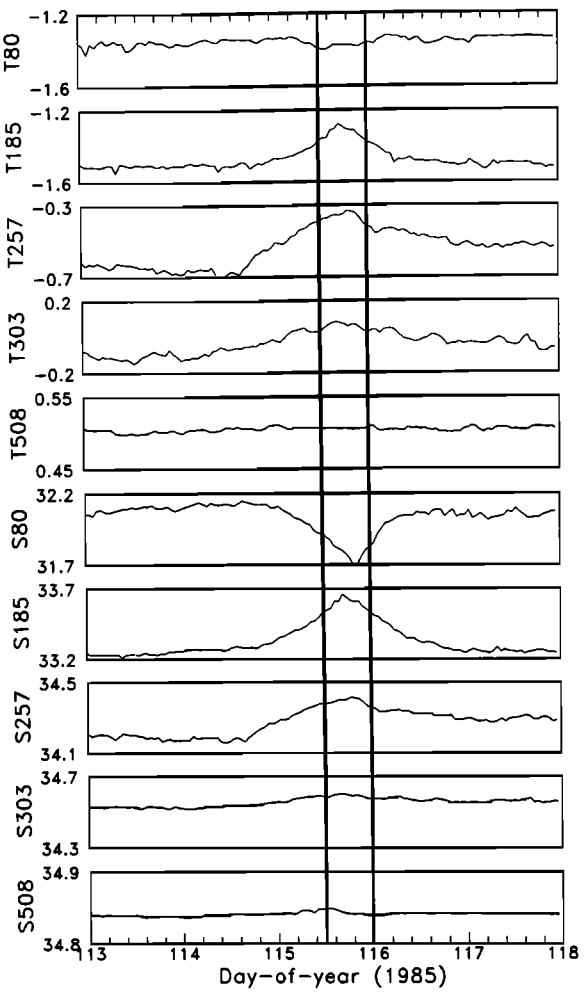

Fig. 4. Time series of hourly averaged temperature and salinity from moored sensors. Vertical lines indicate the position of the eddy, based on current speed at 115 m.

112.0 and t = 116.8, the end of AIWEX microstructure profiling. The dissipation rate of turbulent kinetic energy, ε, is calculated from the microscale shear by (assuming isotropy)

$$\varepsilon = 7.5\nu\langle u_z^2\rangle \quad (1)$$

where ν is the kinematic viscosity of seawater, about 1.8×10^{-6} m^2 s^{-1} at T = 0°C, and $\langle u_z^2\rangle$ is the total shear variance within a chosen depth range. In practice, the shear variance is the integral of the shear spectrum for wavelengths between the Kolmogorov microscale, $\lambda_k = 2\pi(\nu^3/\varepsilon)^{1/4}$, and 0.5 m, the latter being the approximate scale at which the profiler couples with the horizontal flow and therefore fails to measure true shear. Some contamination occurs at low wave numbers due to instrument wobbling and temperature sensitivity of the shear probes. The approximate noise level for ε, based on the smallest values recorded outside the eddy, is about 4×10^{-11} W kg^{-1} (m^2 s^{-3}). No dissipation rates are available above 20 m because the instrument takes several seconds to stabilize following its release. Since the unstratified surface layer at this time is only 15–20 m thick, we are unable to study the mixing layer turbulence.

Dissipation rate profiles (Figure 6) were averaged for four regions of the eddy determined by the ADCP current speed at 115 m. In all regions the dissipation rate above 70 m is significantly above the noise level, while enhanced dissipation rates are also found near 60 and 180 m in the first region (the eddy "core" between t = 115.5 and 116.0). The near-surface dissipation layer extends well into the pycnocline below the surface unstratified layer in all regions, including the far field, and is presumably due to instabilities in the internal wave field generated by stress at the ice/water interface. The velocity field of the eddy is just visible in the ADCP currents at 30 m; therefore the presence of turbulence from the surface to 70 m indicates that a vertical turbulent exchange of momentum between the mixed layer and the

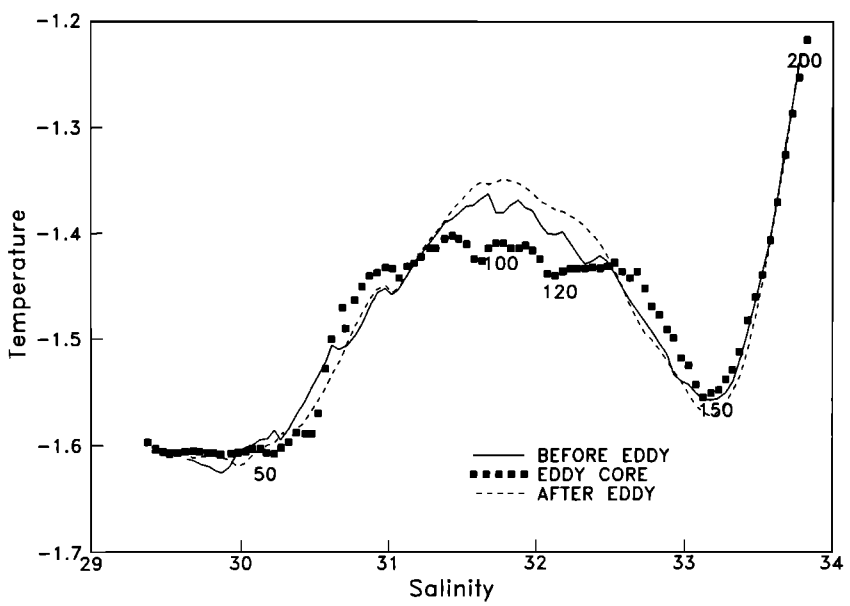

Fig. 5. Temperature versus salinity prior to the eddy, within the eddy core, and after the eddy. Approximate depths within the eddy core are indicated.

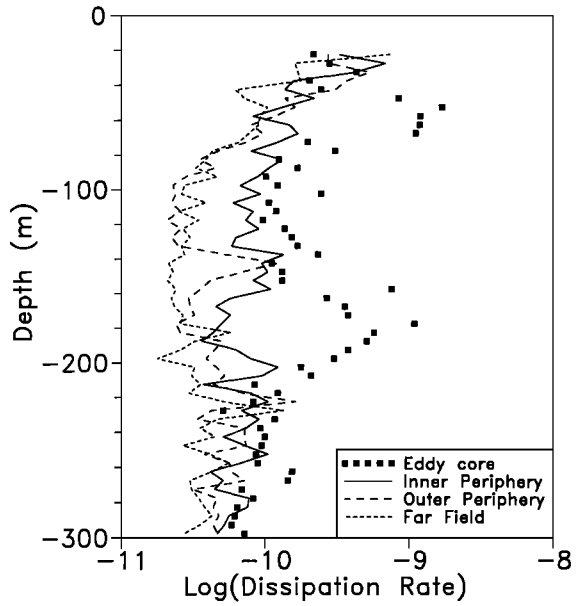

Fig. 6. Profiles of dissipation rate, averaged for four regions based on azimuthal velocity at 115 m: Solid squares denote eddy core, $r < r_0$; solid curve denotes inner periphery, $r > r_0$, $|v_{max}| > 0.2$ m s^{-1}; long-dashed curve denotes outer periphery, $0.1 < |v_{max}| < 0.2$ m s^{-1}, and short-dashed curve denotes far field, $|v_{max}| < 0.1$ m s^{-1}.

underlying velocity field is occurring, although ε is only 4×10^{-10} W kg^{-1} at 20 m, near the base of the mixed layer. The implied interaction between the eddy's velocity field and the ice is consistent with the observed perturbation to the mean ice drift track as the eddy is crossed, seen as a stagnation of ice drift between t = 115.25 and 115.5 (Figure 1), even though no concurrent wind stress change was observed. However, the vertical momentum flux based on the measured dissipation rates and vertical shears is very small, so that the dynamical reason for this apparent eddy/ice coupling is unclear.

3. Discussion

3.1. *Estimates of Eddy Size and Translational Motion*

It is difficult to accurately estimate the horizontal extent of small Arctic eddies because of the irregular drift track of the ice, and the possibility of significant translational motion of the eddy. However, we show below that with two assumptions about the present eddy, namely, that it is axisymmetric and has a core in solid body rotation, we can obtain an estimate of the core radius, the total radius, and the eddy's translational motion. The above assumptions are based on *D'Asaro*'s [1988*a*] findings from helicopter surveys of an anticyclonic eddy found near the AIWEX camp.

The local current magnitude maxima near z = 115 m at t = 115.5 and 116.0 are two crossings of the radius of maximum velocity, $r = r_0$, since the isopycnal displacements between these two points indicate a closer approach to the eddy axis (see Figures 3 and 4). With the assumption that the eddy core, defined as $r < r_0$, is in solid body rotation, we estimate r_0 from a comparison of ADCP measurements with velocities calculated from cyclogeostrophy and measured horizontal density gradients. From the hydrographic data (Figures 3 and 4) the closest approach to the eddy axis is near t = 115.7; the maximum azimuthal velocity, v_a, from the ADCP record at this time is 0.26 m s^{-1}, compared with $v_a \approx 0.38$ m s^{-1} at t = 116.00. The solid body assumption, $v_a \propto r$ for $r < r_0$, implies that the closest approach to the axis is therefore $r \simeq 0.7r_0$, the radial separation of the hydrographic profiles for t = 115.7 and 116.0 is $0.3r_0$, and the velocity determined from a comparison of the two hydrographic profiles applies to $r \simeq 0.85r_0$.

The gradient wind balance for an axisymmetric velocity field under the Boussinesq approximation on an f plane is

$$\frac{\partial \rho}{\partial r} = \frac{\rho_0}{g}\left[\frac{2v_a}{r} + f\right]\frac{\partial v_a}{\partial z} \tag{2}$$

where $\rho(r, z)$ is the density, ρ_0 is a reference density, f is the Coriolis parameter, and v_a is positive for a cyclonic eddy. The assumption of constant f is reasonable given the small horizontal scale of the eddy. The ADCP data can be used to estimate v_a and $\partial v_a/\partial z$, while $\partial \rho$ is given by the horizontal density difference between the two hydrographic profiles at t = 115.7 and 116.0. Equation (2) can then be solved for r_0 at each depth for which the ADCP measurements are independent. We restrict the analysis to the range $64 < z < 180$ m (16 independent depths), where the azimuthal velocities are much higher than the probable non–eddy related baroclinic currents. Three more estimates around z = 115 m are excluded because the small vertical shear at this depth prevents a reliable solution to (2). The average of the 13 remaining estimates of r_0 is 7 km, with a standard deviation of 2 km. There is no significant depth dependence in $r_0(z)$. Significant isopycnal displacements below 270 m are not correlated with large current shear because N is small, so that $\partial \rho/\partial r$ is also small.

The measured ice drift track, the difference in the current direction between the two crossings of r_0 (see Figure 1), and the axisymmetric assumption imply a mean eddy translation velocity v_{trans} of about 0.08 m s^{-1} toward the north or northwest. From repeated observations of particular eddies during AIDJEX, *Manley and Hunkins* [1985] suggest that eddies move with the Beaufort gyre circulation on long time scales, and are coupled on shorter time scales (several days) to wind forcing, a result which *D'Asaro* [1988*a*] also found from repeated surveys of an anticyclonic eddy near the AIWEX camp. The present study suggests that the eddy is moving across the Beaufort gyre streamlines [*Newton et al.*, 1974], and also approximately perpendicular to the ice drift. However, prior to entering the eddy's velocity field, there was a mean northward flow of about 0.1 m s^{-1} present in the upper 300 m, while after leaving the eddy this mean flow was absent (Figure 1). The eddy therefore appears to be moving northward at the edge of a larger scale feature in the dynamic topography, although the lack of hydrographic data below 400 m precludes an adequate assessment of the large-scale geostrophic flow field. Straining of the eddy by a larger-scale horizontal shear field may also invalidate the axisymmetric assumption.

An independent estimate for v_{trans} can be made from the temporal lags observed as the horizontal array of moored temperature sensors near 250 m drifted through the eddy. The array configuration is shown in Figure 2 and the signals at the three outer sensors are shown in Figure 7. Eddy translation relative to the ice was first estimated as the array entered the eddy core, then again as it left the eddy core. For

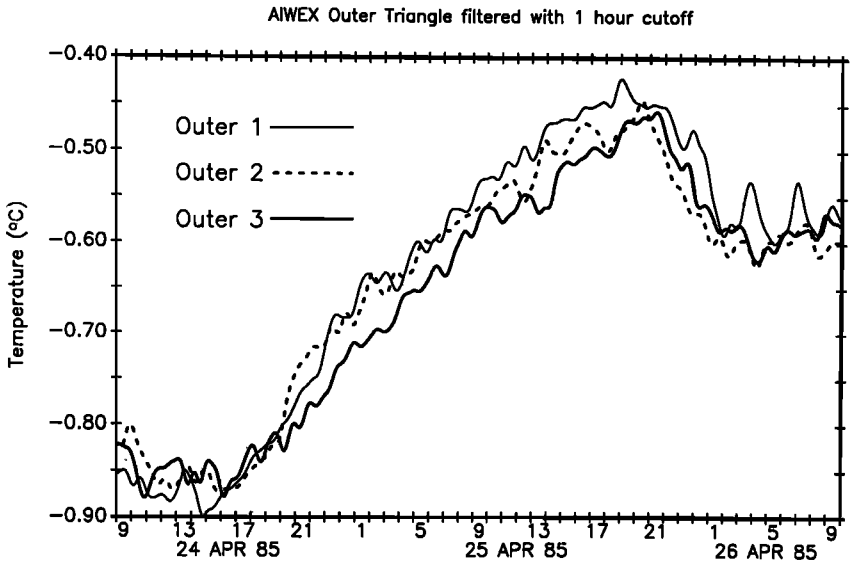

Fig. 7. Examples of temporal lags between 250-m temperature sensors during the transect across the eddy. Locations of sensors are shown in Figure 2.

each case, the direction and speed of eddy motion was determined by minimization of the speed variance from all available sensor pairs as a function of eddy edge orientation. The ice velocity was then added to give the absolute eddy translation velocity. The two estimates of v_{trans} are 0.08 m s^{-1} toward NNE, and 0.06 m s^{-1} toward NNW. Potential sources of error include ignoring eddy curvature, internal wave displacement of isopycnals, and small vertical excursions of the sensors from current drag on the moorings. However, the agreement with the previous estimate based on assumed eddy geometry and cyclogeostrophy suggests that we have a reasonable understanding of the eddy size and motion.

If v_{trans} is assumed constant from $t = 116.0$ to $t = 116.85$, the approximate limit of currents attributable to the eddy, the total radius, r_1, is about 6 km greater than r_0. These results are summarized in Figure 8, which shows the ice drift relative to the eddy center, assuming an eddy translation velocity of 0.08 m s^{-1} toward true north.

With the above estimate of r_0, the Rossby number evaluated at 115 m, $R_v = 2|U_{max}|/fr_0 \simeq 0.75$, i.e., the centrifugal correction to geostrophy in (2) will be important over much of the depth range of the eddy. The aspect ratio of previously documented Arctic SCVs appears approximately constant, with a Burger number, $B = (NH/fL)^2$ of about unity [*D'Asaro*, 1988*a*], where H and L are characteristic vertical and horizontal length scales, respectively. Using the separation between the depths of maximum isopycnal displacement, about 100 m, for H, $N = 0.01$ s^{-1}, and $L = 2r_0$, $B \simeq 0.24$, although with the above uncertainty of ±2 km in r_0, $0.15 < B < 0.5$, comparable to *D'Asaro*'s [1988*a*] tabulated values. However, where $N(r, z)$ varies significantly, as in the present study, it is difficult to estimate H and therefore B.

3.2. *Eddy Energy Balance*

A time scale for eddy decay is

$$t_\varepsilon = E_{tot}/\varepsilon_{tot} \tag{3}$$

where $E_{tot} = KE_{tot} + APE$ is the total energy anomaly of the eddy, and ε_{tot} is the volume-integrated dissipation rate. KE_{tot} is the volume-integrated kinetic energy,

$$KE_{tot} = \int_V \tfrac{1}{2}\rho v_a^2\, dV \tag{4}$$

where V is the volume of the eddy. The APE is the available potential energy of the eddy, calculated numerically following the suggestions of *Hebert* [1988] for the model eddy discussed above. The eddy is divided horizontally into 85

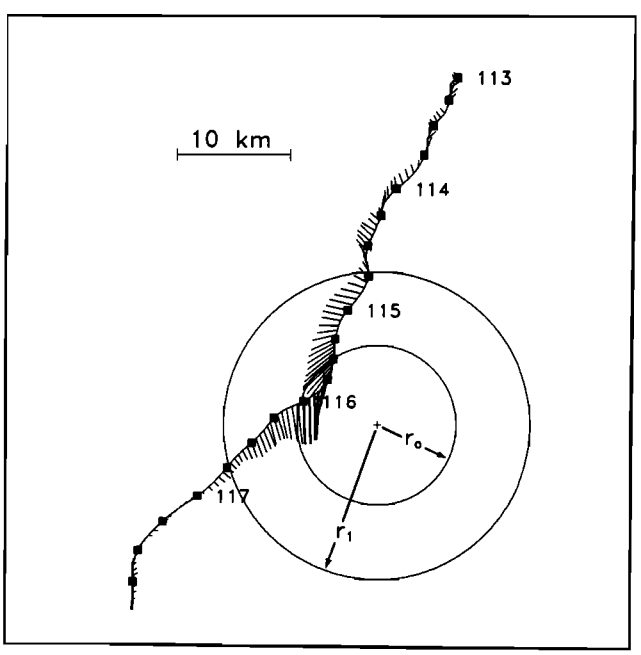

Fig. 8. Camp drift relative to the eddy, assuming the eddy is drifting northward at 0.08 m s^{-1}. Vectors indicate absolute currents at 115 m from the ADCP.

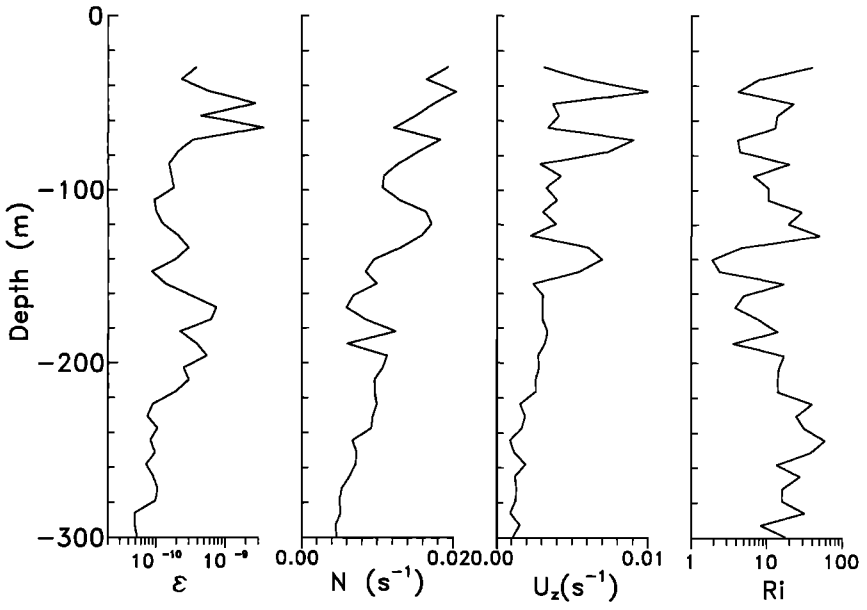

Fig. 9. Dissipation rate ε, buoyancy frequency N, velocity shear magnitude U_z, and Richardson number Ri, averaged over eddy core.

annulae from the center to the far field for 60 depth intervals from the surface to 300 m, i.e., encompassing the entire depth range in which isopycnal displacements are significant, for a total of 5100 annulae. The outermost annulae represent the background density field for a basin of finite radius into which the eddy would gravitationally collapse if its velocity field was removed. The volume and mean density of each annulus are determined, and the thickness that each annulus would have after spreading into a uniformly thick disc throughout the basin is calculated. The 5100 resultant discs are then reordered in depth to a monotonic density profile, with the *APE* being the difference between the potential energies of the original and reordered states. While the best estimate of the *APE* is for collapse of the eddy into an infinitely large basin, because of round-off errors in the numerical computation, the *APE* estimate diverges as the horizontal scale of the far field is increased beyond a certain value [*Hebert*, 1988]. We therefore calculate the *APE* over a range of far-field radii, adjusted by increasing the width of the outermost annulae, then take as the best estimate the asymptotic limit of *APE* prior to numerical divergence. To study the uncertainty in the *APE* estimate, the number of radial and depth bins was modified, and a check made of the final integrated volume of the discs compared with the volume of the model basin. From these studies, numerical errors may be 20% of the calculated *APE*. The model axisymmetric eddy with $r_0 = 7$ km and total radius $r_1 = 13$ km, and linear velocity profiles above and below 115 m decaying to zero at 30 and 270 m, has a total kinetic energy of about 1.5×10^{12} J and an *APE* of about 2.9×10^{12} J, for a total energy anomaly of 4.4×10^{12} J. The resultant "energy" Burger number, $B_E = KE_{tot}/APE$ is about 0.5, significantly less than the typical values quoted by *D'Asaro* [1988*a*]. Various other functional forms for the eddy's radial velocity dependence still produce values of $B_E < 1$.

Dissipation rates in the model eddy are assumed to be a constant value in the eddy core (the mean value from measurements for $r < r_0$), and either zero or at the noise level for $r > r_0$. The volume-integrated dissipation rate is between 8.4×10^3 and 1.8×10^4 W depending on whether noise level dissipations are set to zero or as measured, giving a decay time scale t_ε of about 10 years. This decay time scale is insensitive to errors in r_0 and r_1 because of the simple spatial dependence assumed for $\varepsilon(r, z)$. We emphasize that t_ε is applicable only to the eddy as observed: Time-dependent external conditions, such as higher internal wave shear variance leading to a greater probability of mixing, might lead to much faster time-averaged decay rates than were observed.

The vertical shears associated with the eddy velocity field suggest that shear instability is a possible cause of the subsurface dissipation rate maxima (Figure 6). Hourly averages of ADCP shear magnitude $[U_z]$ and buoyancy frequency N from the APS, averaged vertically over 8 m, are combined to create a transect of Richardson number, $Ri = N^2/|U_z|^2$. It is usual to assume that a low value of Richardson number, less than $\frac{1}{4}$, implies that initially infinitesimal perturbations of the density field can be amplified by the local shear until a gravitationally unstable overturn is created. However, when the averaging scales are larger than a typical mixing event, or after the outer vertical scale of the turbulence has decayed to below the averaging scale for Ri, mean Richardson numbers greater than $\frac{1}{4}$ may still be accompanied by significant mixing [*Padman and Jones*, 1985]. Averaged Richardson number is therefore used qualitatively only, to indicate the most likely locations of mixing events.

Values of $Ri < 10$ are found only in the eddy core. Vertical profiles of $|U_z|$, N, Ri, and ε averaged over all profiles within the core are shown in Figure 9. There is no obvious relationship between sites of high ε and low Ri, although there is a suggestion that large dissipation rates are related to regions of small mean shear (the upper region of high ε occurs between zones of high shear, while the lower region is bounded above by a high shear zone). One plausible scenario is that the observed regions of large ε are the remnants of recent, much more energetic mixing events at

TABLE 1. Properties of the AIWEX Camp Eddy

Parameter	Value
Depth of maximum velocity	115 m
Depth range for $\|U\| > 0.05$ m s^{-1}	$40 < z < 250$ m
Radius of maximum velocity, r_0	7 ± 2 km
Maximum radius, R_{max}	13 ± 4 km
Rossby number $R = \|U\|_{max}/r_0 f$	0.75
Stratification Burger number, B	0.24
Total kinetic energy, KE_{tot}	1.5×10^{12} J
Available potential energy, APE	2.9×10^{12} J
Energy Burger number, B_E	0.5
Total energy, $E_{tot} = KE_{tot} + APE$	4.4×10^{12} J
Volume-integrated dissipation rate, ε_{tot}	$(1.3 \pm 0.5) \times 10^4$ W
Dissipation time scale, $t_\varepsilon = E_{tot}/\varepsilon_{tot}$	10 years

these depths, which had locally homogenized the momentum. A corollary to this hypothesis is that the time-averaged dissipation rate is much larger than the measured rate because of the importance of such intermittent but energetic mixing events. Correspondingly, the mean dissipation decay time scale will be much shorter than suggested above.

A summary of the eddy's properties is given in Table 1.

3.3. *Interaction of the Eddy With the Environment*

3.3.1. *Surface layer dynamics.* A transect of salinity at 10 m depth from the APS (Figure 10) shows a decrease of about 0.4 practical salinity units (psu) over the eddy, concurrent with an increase in T, which remains near 0.01°C above the freezing point for the observed salinities. Relatively fresh water is produced by the melting of ice, and the production rate increases with the stress at the ice/water interface [*McPhee et al.*, 1987], since the supply of heat from the warmer water underlying the surface layer depends on the intensity of turbulent mixing in the surface layer. While no dissipation rates can be estimated for $0 < z < 20$ m because of instrument motion, the averaged dissipation rate profiles below this depth (Figure 6) suggest a similar turbulent stress near the ice/water interface for all four averaging regions, including the far field, which implies similar freshwater production rates within and outside the eddy. However, the stress applied by the ice to the upper edge of a nontranslating cyclonic SCV produces an inward mass flux in the surface layer. This flow is horizontally convergent ($\nabla_H \mathbf{u} = \{\partial u/\partial x + \partial v/\partial y\} < 0$) for $r < r_0$, while for $r > r_0$, $\nabla_H \mathbf{u}$ may be either positive or negative depending on the radial decay rate of azimuthal velocity. For our model eddy with v_a decaying linearly for $r_0 < r < r_1$, $\nabla_H \mathbf{u}$ is positive (divergent) in this region, although the extension of the freshwater pool to $r > r_0$ suggests that the flow is actually convergent. For $r > r_1$, the flow is expected to be nondivergent on scales smaller than the coherence scales of the wind stress. The result of this flow pattern is to advect fresh surface water into the eddy core; conservation of mass implies a downwelling to balance $\nabla_H \mathbf{u}$. T. Manley (personal communication, 1989) has suggested that the fresh water represents a pooling of fluid which is too buoyant to be downwelled.

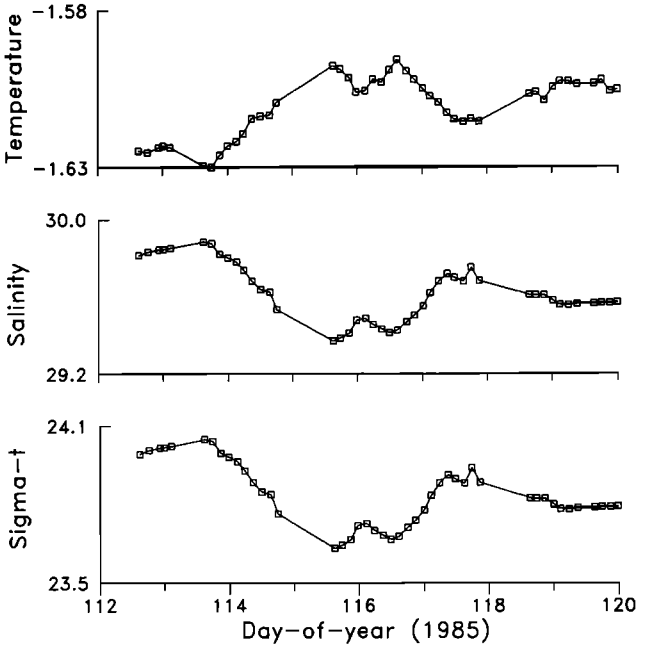

Fig. 10. Temperature, T, salinity, S, and density, σ_t, at 10 m depth. The eddy core is between $t = 115.5$ and $t = 116.0$.

The addition of an eddy translation velocity relative to the ice introduces an asymmetry into the horizontal divergence field, and hence to the distribution of upwelling velocity. More importantly, the higher surface stresses associated with relative ice motion increase the rate at which momentum is lost from an eddy, and *Ou and Gordon* [1986] find a decay time scale of only a few days after an initially surface-intensified eddy in open water moves under the ice cover. This occurs not only through frictional losses at the ice/water interface, but also through the vertical advection required to balance the horizontal divergences. Both the low observed near-surface dissipation rates and the assumed long life time of the eddy indicate that the momentum loss at the surface was negligible at the time the eddy was observed. It is probable that part of the stress balance in the surface layer is the radial pressure gradient, established initially by the surface stress, and enhanced by the resultant radial density gradient.

3.3.2. *Critical layer absorption of internal wave momentum.* Critical layer absorption of internal wave momentum can occur where the intrinsic frequency of a wave, $\omega_i = \omega - \mathbf{k} \cdot \mathbf{u}$, becomes equal to $\pm f$. Internal waves generated by form drag resulting from the relative motion of under-ice topography are expected to have phase velocities, $c_p = \omega/|k|$, approximately equal to the ice velocity. In the Canada Basin, away from eddies and coastal boundary currents, c_p is usually greater than $|\mathbf{u}|$ at all depths; therefore the wave energy may penetrate to the seabed. However, near energetic features, wave absorption may occur much closer to the surface, depositing momentum into the upper pycnocline. Furthermore, the selective absorption of wave numbers with components in the direction of the flow provides a mechanism for maintenance or even growth of the kinetic energy anomaly, since the absorbed momentum is always of the same sign as the existing velocity; wave momentum which could deaccelerate the flow either passes through the region of high current speed, or is reflected because of variations in buoyancy frequency and vertical shear.

In an SCV, the effect of critical layer absorption is to apply a torque in the direction of eddy rotation, i.e., in the absence of competing decay processes, the eddy rotation speed would increase. To quantify this effect, we estimate the

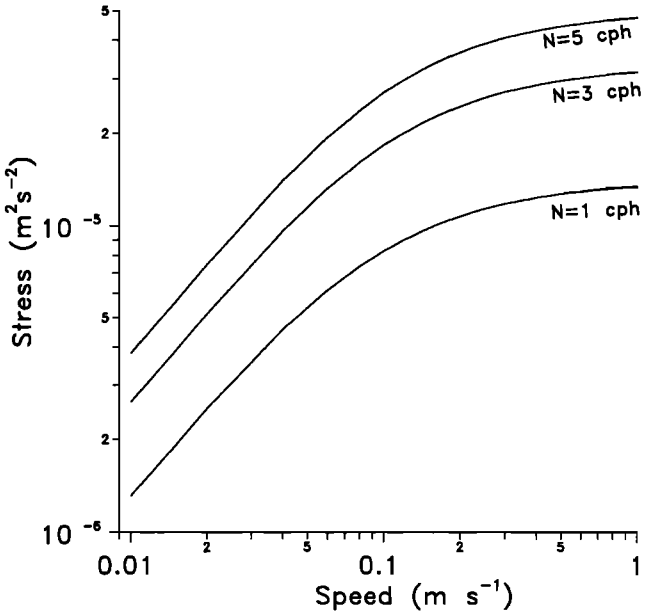

Fig. 11. Momentum flux lost to critical layer absorption versus maximum current speed (from (5)), for a range of $\langle N \rangle$ characteristic of the Arctic density stratification.

vertical flux of momentum through a model internal wave field which differs from the form proposed by *Munk* [1981] only in that the frequency spectrum is proportional to ω^{-1} rather than ω^{-2} [*Levine et al.*, 1987], based on the moored temperature and conductivity data. Other parameters are obtained from moored coherence estimates [*Levine*, 1990]. We follow the basic arguments of *Ruddick* [1980] to estimate the fraction of the total downward momentum flux near the surface which is absorbed given a maximum subsurface velocity of $\bar{u}$ m s^{-1}. The lost momentum flux, F_{lost}, is given by a nonseparable triple integral in ω, horizontal wave number, and the relative angle between the current and the wave momentum [*Ruddick*, 1980, equation (10)]. This integral reduces approximately to an integral in ω only.

$$F_{\text{lost}} \approx \frac{E_0}{N_0 U \ln(2N/f)} \int_f^N d\omega \cdot \{[\omega^2(1+U)^2 - 2\omega f + f^2(1-U^2)]^{1/2} - \omega + f\}(\omega^2 - f^2)^{-1/2} \quad (5)$$

where E_0 is the kinetic energy density, 1.5×10^{-4} m^2 s^{-2}, $N_0 = 0.0052$ s^{-1}, N is the local buoyancy frequency, and $U = \bar{u}/\hat{u}$, where $\hat{u} = N_0 b/\pi j*$, b is a depth scale, 1300 m, and $j*$ is the equivalent number of modes in vertical wave number space, $j* \simeq 30$ from *Levine* [1990]. Equation (5) can be evaluated numerically, and the results are shown in Figure 11 for a range of N spanning the observed stratification in the Canada Basin.

For the observed maximum speed in the SCV, $\bar{u} = 0.38$ m s^{-1}, $F_{\text{lost}} \simeq 2.5 \times 10^{-5}$ m^2 s^{-2}. Assuming this absorption occurs uniformly from the base of the mixed layer at 20 m to the depth of maximum velocity near 115 m, an acceleration of $a_{IW} = 2.5 \times 10^{-7}$ ms^{-2} is implied, corresponding to a time scale $\bar{u}/2a_{IW} \approx 10$ days. Comparable absorption may occur in the lower section of the eddy by absorption of upward propagating waves. *Kunze and Müller* [1989] argue that, at least for a relatively simple two-dimensional geometry, the important balance in the momentum equation

$$\frac{Du}{Dt} - fv = \frac{\partial \langle u'w' \rangle}{\partial z} \quad (6)$$

where u is aligned with the local shear and $\partial\langle u'w'\rangle/\partial z$ is the divergence of the wave Reynolds stress, is actually between the stress divergence and an "Ekman" flow, v, normal to the geostrophic flow. While their results are not formally applicable to the complex, three-dimensional eddy geometry, this interpretation implies a modification of the SCV's horizontal scale, L, with an estimated time scale of

$$t_E = LHf/F_{\text{lost}} \quad (7)$$

where H is a vertical length scale. Then for $L = 5$ km, $H = 100$ m, and the above value of F_{lost}, $t_E \simeq 30$ days. Critical layer absorption therefore dominates the observed turbulent dissipation in the kinetic energy budget, regardless of whether the principal balance in (6) is with the acceleration or an Ekman flow term. However, a more plausible hypothesis, consistent with the suggestion in section 3.2 that the depths of enhanced dissipation rates are simply the remnants of much more energetic mixing events, is that such accelerations are limited by intermittent instability in the eddy's sheared velocity field. We propose, therefore, that the time-averaged dissipation rate is sufficiently large to balance the rate of absorption of internal wave momentum flux.

Absorption may be at least partially offset by reradiation through the collapse of developing instabilities in the mean flow, while reflection by the vertical gradients in N will reduce the available wave momentum flux for absorption deeper in the eddy. As well, the eddy diameter and height are comparable to the larger horizontal and vertical wavelengths in the model internal wave field, complicating the mechanisms of mean shear/wave interaction. However, even a very inefficient transfer of momentum from the internal waves to the mean flow would exceed the observed kinetic energy dissipation rates. Also note that if the vertical momentum flux has a peak at phase velocities comparable to the relative ice motion, then variability in ice drift will be seen as a variation in the depth of optimum absorption. That the two high-dissipation rate peaks near 60 and 180 m correspond to eddy azimuthal velocities between 0.1 and 0.2 m s^{-1}, comparable to mean ice drift rates, may be fortuitous, but suggests that this mechanism is worthy of further research.

4. Summary

A study of a cyclonic, baroclinic, submesoscale eddy which was crossed by the AIWEX ice camp in the Canada Basin in April 1985 has shown the following.

1. The eddy has a radius of maximum velocity, r_0, of about 7 ± 2 km, and a total radius of about 13 km. Azimuthal velocity decays from a maximum at about 115 m depth, to almost zero at 30 m and 270 m.

2. The water in the mixed layer above the eddy is anomalously fresh, consistent with the pooling and entrapment of fresh water by a horizontally convergent surface layer velocity field.

3. At the time it was observed, the eddy was moving

approximately northward at 0.08 m s^{-1}, perpendicular to both the basin-scale dynamic topography and the ice motion, but consistent with measured currents prior to the camp's passage through the eddy.

4. Dissipation rates were above the instrument's noise level in the upper 70 m throughout the transect, and near 60 and 180 m within the eddy core ($r < r_0$). Since the subsurface dissipation maxima do not correspond to regions of low Richardson number, but are coincident with low shear, the observed dissipation rates appear to be the remnants of more energetic mixing events.

5. The total energy of the eddy is about 5×10^{12} J, which, given the observed dissipation rates, suggests a decay time scale of $O(10)$ years.

6. Estimates of the rate of critical layer absorption of downward propagating internal wave momentum indicate that this absorption may be an important term in the total energy balance of the eddy, given the low observed dissipation rates.

Validation of our hypothesis that the eddy's vorticity field is maintained by critical layer absorption of internal gravity wave momentum would require repeated observations of the same eddy over a period of several months, a particularly challenging problem in ice-covered seas. However, the mechanism does help explain the long lives of the Canada Basin eddies, and provides the means to maintain an energetic eddy even while its *TS* signature is eroded by turbulent diffusion.

Acknowledgments. We acknowledge valuable discussions with E. D'Asaro, T. Manley, E. Kunze, and J. Barth. The comments of an anonymous reviewer were also appreciated. VACM data was provided by C. A. Paulson. This work was supported by the Office of Naval Research, contract numbers N00014-84-C-0218 and N00014-87-K-0009 (L.P., M.L., T.D.), N00014-90-J-1077 (J.M.), and N00014-85-K-0010 (R.P.).

REFERENCES

Caldwell, D. R., T. M. Dillon, and J. N. Moum, The rapid-sampling vertical profiler: An evaluation, *J. Atmos. Oceanic Technol.*, *2*, 615–625, 1985.

D'Asaro, E. A., Observations of small eddies in the Beaufort Sea, *J. Geophys. Res.*, *93*, 6669–6684, 1988*a*.

D'Asaro, E. A., Generation of submesoscale vortices: A new mechanism, *J. Geophys. Res.*, *93*, 6685–6694, 1988*b*.

Fields, E., Towards a plausible origin of the AIWEX lenses, M.S. dissertation, Oreg. State Univ., Corvallis, 1988.

Griffiths, R. W., and P. F. Linden, Laboratory experiments on fronts, *Geophys. Astrophys. Fluid Dyn.*, *19*, 159–187, 1982.

Hebert, D., The available potential energy of an isolated feature, *J. Geophys. Res.*, *93*, 556–564, 1988.

Hunkins, K. L., Subsurface eddies in the Arctic Ocean, *Deep Sea Res.*, *21*, 1017–1033, 1974.

Killworth, P. D., and M. E. Stern, Instabilities on density-driven boundary currents and fronts, *Geophys. Astrophys. Fluid Dyn.*, *22*, 1–28, 1982.

Kunze, E., and P. Müller, The effect of internal waves on vertical geostrophic shear, paper presented at the Fifth 'Aha Huliko'a Hawaiian Winter Workshop, Dept. of Oceanogr., Univ. of Hawaii, Honolulu, 1989.

Levine, M. D., Internal waves under the Arctic ice pack during AIWEX: The coherence structure, *J. Geophys. Res.*, *95*, 7347, 1990.

Levine, M. D., S. R. Gard, and J. Simpkins, Moored temperature and conductivity observations during AIWEX, *Ref. 86-9*, 195 pp., Coll. of Oceanogr., Oreg. State Univ., Corvallis, 1986.

Levine, M. D., C. A. Paulson, and J. H. Morison, Observations of internal gravity waves under the Arctic pack ice, *J. Geophys. Res.*, *92*, 779–782, 1987.

Manley, T. O., and K. L. Hunkins, Mesoscale eddies of the Arctic Ocean, *J. Geophys. Res.*, *90*, 4911–4930, 1985.

McPhee, M. G., G. A. Maykut, and J. H. Morison, Dynamics and thermodynamics of the ice/upper ocean system in the marginal ice zone of the Greenland Sea, *J. Geophys. Res.*, *92*, 7017–7031, 1987.

McWilliams, J. C., Submesoscale coherent vortices in the ocean, *Rev. Geophys.*, *23*, 165–182, 1985.

McWilliams, J. C., Vortex generation through balanced adjustment, *J. Phys. Oceanogr.*, *18*, 1178–1192, 1988.

Morison, J. H., M. G. McPhee, and G. A. Maykut, Boundary layer, upper ocean, and ice observations in the Greenland Sea marginal ice zone, *J. Geophys. Res.*, *92*, 6987–7011, 1987.

Munk, W. H., Internal waves and small-scale processes, in *Evolution of Physical Oceanography*, edited by B. A. Warren and C. Wunsch, pp. 264–291, MIT Press, Cambridge, Mass., 1981.

Newton, J. L., K. Aagaard, and L. K. Coachman, Baroclinic eddies in the Arctic Ocean, *Deep Sea Res.*, *21*, 707–719, 1974.

Ou, H. W., and A. L. Gordon, Spin-down of baroclinic eddies under sea ice, *J. Geophys. Res.*, *91*, 7623–7630, 1986.

Padman, L., and T. M. Dillon, Vertical heat fluxes through the Beaufort Sea thermohaline staircase, *J. Geophys. Res.*, *92*, 10,799–10,806, 1987.

Padman, L., and T. M. Dillon, On the horizontal extent of thermohaline steps in the Canada Basin, *J. Phys. Oceanogr.*, *18*, 1458–1462, 1988.

Padman, L., and I. S. F. Jones, Richardson number statistics in the seasonal thermocline, *J. Phys. Oceanogr.*, *15*, 844–854, 1985.

Ruddick, B. R., Critical layers and the Garrett-Munk spectrum, *J. Mar. Res.*, *38*, 135–145, 1980.

T. Dillon, M. Levine, and L. Padman, College of Oceanography, Oregon State University, Corvallis, OR 97331.

J. Morison, Applied Physics Laboratory, University of Washington, Seattle, WA 98195.

R. Pinkel, Scripps Institution of Oceanography, La Jolla, CA 92093.

(Received October 12, 1989;
accepted December 7, 1989.)